Hurst Exponent and IntraPartum Fetal Heart Rate: Impact of Decelerations

Patrice Abry[(1)], Stéphane G. Roux[(1)], Václav Chudáček[(1)],
Pierre Borgnat[(1)], Paulo Goncalvès[(2)], Muriel Doret[(3)]
[(1)] Physics Dept. ENS Lyon, CNRS, firstname.lastname@ens-lyon.fr
[(2)] Comp. Sciences Dept. ENS Lyon, INRIA, firstname.lastname@ens-lyon.fr,
[(3)] Hôpital Femme-Mère-Enfant, HCL, University of Lyon, muriel.doret@chu-lyon.fr
Work supported by ANR BLANC 2010 FETUSES 18535 and HCL-HFME PHRC grant.

Abstract

Intrapartum fetal heart rate monitoring constitutes an important stake aiming at early acidosis detection. Measuring heart rate variability is often considered a powerful tool to assess the intrapartum health status of fetus and has has been envisaged using various techniques. In the present contribution, the power of scale invariance parameters, such as the Hurst exponent and the global regularity exponent, estimated from wavelet coefficients of intrapartum fetal heart rate time series, to evaluate the health status of fetuses is quantified from a case study database, constituted at a French Academic Hospital in Lyon. Notably, the ability of such parameters to discriminate subjects incorrectly classified according to FIGO rules as abnormal *will be discussed. Also, the impact of the occurrence of decelerations identified as* complicated *by obstetricians on the values taken by Hurst parameter is investigated in detail.*

1 Motivation

Fetal Heart Rate Surveillance. Cardiotocography (CTG) – monitoring of fetal heart rate (FHR) and uterine contractions (TOCO) – has been, since the sixties used routinely by obstetricians to detect antepartum as well as intrapartum fetal hypoxia (cf. e.g., [5]). Notably, intrapartum FHR surveillance constitutes a crucial task, whose stakes are reduction of fetal and neonatal mortality and morbidity due to asphyxia. The evaluation of FHR status in clinical setting mostly relies on the evaluation of macroscopic morphological beat-per-minute (bpm) time series features, notably those defined by the FIGO guidelines [11]. Such guidelines, aiming at detecting almost surely any case of fetal asphyxia (high sensitivity) are however also known to yield a low specificity. Such false positives in turn induce a high number of operative deliveries, with potentially severe consequences for the mother and the newborn, that may actually not have been needed. Increasing specificity thus constitutes a challenging task in intrapartum FHR analysis.

Fetal Heart Rate Analysis. Beyond FIGO features, many different characterizations of FHR have been considered, cf. e.g., [21, 14] for reviews and comparisons, a number of them focusing on the notion of FHR *variability*. In practice, variability is often measured as the largest difference (oscillation) that can be measured within a time window of size a:

$$V_a(t) = \sup\{|X(u) - X(v)|\}, \quad (u,v) \in [t - a/2, t + a/2]^2, \tag{1}$$

where $X(t)$ denotes the (regularly sampled) FHR time series in bpm. Classically, Short term Variability (STV) and Long term Variability (LTV) (as defined in [7, 11] respectively) correspond to specific choices of analysis windows ($a = 3.75$s and $a = 60$s, respectively). Most systems for automated CTG evaluation – including current Sisporto 3.5 [3] — are making use of LTV, while the potential of STV for intrapartum FHR surveillance remains controversial. The reader is referred to [4] for a survey on the use of STV intrapartum FHR surveillance and to [20, 19] for interesting discussions. Alternatively, FHR has also been characterized by means of spectrum analysis (cf. e.g., [22, 23]). In essence, it amounts to assuming that FHR time series X can be regarded as (second-order) stationary process, with power spectrum density (PSD) $\Gamma_X(f)$ that measures the contribution of the different frequencies, or frequency bands, to the temporal dynamics of X. Changes in that frequency balance may provide obstetricians with indications of modification in the fetus health status. More recently, the concept of *fractal* (or scale invariance) has been envisaged for FHR characterization (cf. e.g., [10, 9, 18]), providing practitioners with scaling exponents such as the Hurst exponent, or the Hölder exponent, to analyze FHR. Very recently, *multifractal analysis*, a signal processing tool aiming at characterizing the variations along time of the local regularity fluctuations of data, has been shown to have interesting potential for the analysis of HRV in adults [16, 15] or intrapartum FHR [13, 2, 8], yielding a richer variety of

scaling exponents.

Goals and contributions. In that context, the present contribution elaborates on the investigation of the potential benefits of using fractal-type attributes to accurately characterize FHR time series. Namely, the attributes used here are the Hurst exponent H and of the global regularity exponent h_m, as defined in Section 3. These exponents are practically estimated using a wavelet decomposition framework, detailed in Section 3 on a case study database, presented in Section 2, and constructed in French University Hospital *Femme-Mère-Enfant*, in Lyon, under the supervision of the obstetrician in charge of the present research program. Precisely, the contributions presented here are fourfold: First, it is explained how the fractal paradigm provides a natural mean to reconcile time variability and spectrum analysis in a single perspective (cf. Section 3.3); Second, it is shown that H and h_m exponents, when measured along sliding time windows, provide a satisfactory characterization of FHR, both in terms of separating Healthy from Non-Healthy subjects, and in terms of evolution along time (cf. Section 4.1); Third, a careful case study is conducted that enables to split FIGO False Positive into various subclasses, those that can actually be re-classified as healthy by fractal attributes and those for which fractal attributes fail to recognize FIGO False Positive as healthy subjects. These two classes are interpreted in terms of FIGO attributes, the latter class being characterized by *complicated decelerations* (cf. Section 4.2). Fourth, therefore, following the case study examples described in [23], the impact of decelerations on the value taken by Hurst exponents is studied in detail and related to the Health status of the fetus (cf. Section 4.3).

2 DataSet

A subset of a large database collected at French Academic Hospital *Femme-Mère-Enfant*, in Lyon, is used here. Three classes of FHR recordings are set up based on a combination of visual analysis by experts (using the FIGO classification) and objective (umbilical cord pH) evaluation. Each class contains 15 FHR signals, from in total 45 different singleton pregnancies (gestation age between 37 and 42 weeks). The database is documented case-by-case with the umbilical cord artery pH, as well as obstetricians annotations related to Baseline (High, Normal, Low), Variability (Low, Normal), Reactivity (Low, Normal), Decelerations (None, Uniform, Variable and Complicated-Shape). The database is organized into three classes as:

FIGO True Negative (FIGO-TN): normal pH (> 7.30), FIGO classification of CTG as Normal;

FIGO True Positive (FIGO-TN): abnormal pH (< 7.05), FIGO classification of CTG as Pathological;

FIGO False Positive (FIGO-FP): normal pH (> 7.30), FIGO classification of CTG as Pathological.

All FHR signals are collected using the STAN S31 recording device using the direct scalp electrode. FHR recordings are of various lengths (mean 123min [min 43min; max 550min]), they are recorded almost in all cases until a few minutes before delivery. RR-intervals are converted into a regularly sampled FHR time series, in bpm, with sampling frequency $f_s = 8$Hz.

3 Scale invariance and wavelet analysis

3.1 Scale invariance and Hurst exponent

It is now commonly observed that FHR variability time series are well characterized by robust fractal (or scale invariance) properties (cf. e.g. [10, 9, 18, 2, 8]), which leads to assume that X can be considered as a second-order stationary process, with PSD characterized by a algebraic (or power-law) decrease:

$$\Gamma_X(f) \sim C|f|^{-(2H-1)},\ |f| \to 0, \tag{2}$$

where the scaling exponent depends on the so-called Hurst exponent $0 < H < 1$. Such an algebraic PSD decrease also corresponds to an algebraic decrease of the covariance function, instead of the more usual exponential decrease. A classical example of such processes is fractional Gaussian noise (fGn) that requires in addition that data are Gaussian. Note however that there is naturally a practical issue that consists of knowing whether data are better modeled by fGn of by fractional Brownian motion (fBm), which essentially consists of the cumulated sum of fGn. Thus, fBm consists of a non stationary process, whose increments are stationary and that possesses scaling properties equally well described by Hurst parameter. In the wavelet framework detailed below, this distinction no longer needs to be made a priori as the estimation for parameter H works equally well in both cases: When data actually follow a fBm model, the estimated Hurst parameter naturally falls in the range $\hat{H} \in [1, 2)$, instead of the theoretical range $H \in (0, 1)$. Accommodating both fGn and fBm in a same H estimation framework is one of the many advantages of the wavelet based framework for the analysis of scaling properties in data (see [1] for a review).

Further note that, for fGn, the theoretical request that the power-law behavior of Γ_X theoretically holds in the limit of low frequencies $f \to 0$, is, for practical use on real world-data, weakened and assumed to hold over a large *scaling range* $f_m \leq f \leq f_M$, with $f_M/f_m \gg 1$, whose experimental determination conveys per se important information related to analyzed data. Both assumptions (Gaussiannity and $f \to 0$) are not needed for the present study, so that explicit reference to fGn is avoided from now on.

3.2 Wavelet Analysis of Scale Invariance

Wavelet Transform. A mother wavelet $\psi_0(t)$ is a reference pattern with narrow supports in both the time and frequency domains. The analysis wavelet collection $\{\psi_{a,t}(u) \equiv$

$a^{-1/2}\,\psi_0((u-t)/a), a \in \mathbb{R}^+, t \in \mathbb{R}\}$ consists of templates of $\psi_0(t)$, dilated at analysis scale $a > 0$ and shifted at time position t. The wavelet transform coefficients of X are defined as $T_X(a,t) = \int_{\mathbb{R}} X(u)\psi_{a,t}(u)du$. For a complete introduction to wavelet transforms, readers are referred to e.g. [17].

Scale Invariance. It has been shown for the analysis of processes with scaling properties, that their wavelet coefficients accurately and robustly reproduce scale invariance (cf. e.g., [1]). Notably, for processes with power law spectra, as in Eq. (2), it has been shown that:

$$\mathbb{E}T_X(a,t)^2 \simeq a^{2H-1}, a_m \leq a \leq a_M, a_M/a_m \gg 1. \quad (3)$$

In addition, recent advances in the analysis of scaling in data have shown that another quantity plays an important role as it conveys a complementary information to H, the global regularity, related to the lowest Hölder exponent, observed in data, and theoretically defined as [8]): $h_m = \liminf_{a\to 0} \frac{\ln \sup_t |T_X(a,t)|}{\ln a}$, h_m notably differs from H when data are non Gaussian.

The scale invariance parameters H and h_m thus provide relevant descriptors of the scale invariance properties of data.

3.3 Variability versus Scale invariance

Wavelet variability. As discussed in introduction, variability is often measured according to Eq. (1), which shed an interesting first interpretation of Eq. (3) above: The quantity $\mathbb{E}T_X(a,t)^2$ can be read as a measure of variability which implies two major changes compared to the traditional one: First, the oscillation is no longer used and replaced by wavelet coefficient, a quantity bringing robustness and versatility to the practical measure; Second, and even more importantly, variability is not characterized by the value it actually takes at specific analysis scales a (such as in the STV and LTV cases) but instead, it is described by the way it varies when the analysis scale a is varied, hence by exponent H.

Wavelet spectrum. When X is a 2^{nd} order stationary random process, it has been shown [1] that the power of the wavelet coefficients can be related to the data spectrum as $\mathbb{E}T_X(a,t)^2 = \int \Gamma_X(f)a|\Psi_0(af)|^2df$, where Ψ_0 stands for the Fourier transform of ψ_0 and $\mathbb{E}$ for the mathematical expectation. Therefore, the quantity $\mathbb{E}T_X(a,t)^2$ can be interpreted as a (wavelet-based) estimate of the PSD Γ_X, around frequency $f = f_0/a$, and is thus often referred to as the *wavelet spectrum*.

Hurst exponent. The Hurst exponent, via the wavelet quantity $\mathbb{E}T_X(a,t)^2$, therefore reconciles the time variability and spectrum estimation perspectives into a unified framework: The energy balance of wavelet coefficients across scales measures both variability as in the traditional setting, but at all scales jointly (rather than only at $a = 3.75$s or $a = 60$s) and temporal dynamic as spectrum estimation does.

3.4 Estimation

It has also been proposed (e.g. in [1]) that the ensemble average $\mathbb{E}T_X(a,t)^2$ can be relevantly estimated by the corresponding time average: $S(a) = \frac{1}{n_a}\sum_{k=1}^{n_a} T_X(a,k)^2$, where n_a denote the number of $T_X(a,t)$ actually computed at scale a. This enables to perform an estimation of the the scaling exponent α (and thus of the Hurst parameter H) via a linear regression: $\hat{H} = ((\sum_j w_j \ln S(a_j)) + 1)/2$, where weights w_j satisfying $\sum_j w_j \ln a_j \equiv 1$ and $\sum_j w_j \equiv 0$. It has been shown to be a robust and efficient procedure for the estimation of H (see [1]). Along the same line, h_m can be estimated in the same manner from a non-weighted linear regression.

4 Results and discussions

4.1 Classification, constancy along time

Scaling properties of FHR time series are now studied by estimating jointly H and h_m, from the FHR time series of each subject, of each class, in 20min long sliding windows (with 50% overlap), for the last 180min before delivery, whenever available. As illustrated in Fig. 3 below, for FHR time series, the power-law behavior as predicted in Eq. (3) is found to hold between scales $a_j = 3$ (corresponding to 1s) to $a_J = 8$ (corresponding to 64s), which, interestingly, are observed to be closely related to the scales used to measure STV and LTV. Fig. 1 displays, for each time window, the median per class of the $\hat{H}$ (with $\pm$ 1 standard deviation (std) lines) as well as, for the 3 pairs of classes and for each time window, the p-values of Wilcoxon ranksum tests, testing the null hypothesis that there is no difference in median. It shows, first, that the FIGO-TP class exhibit much larger $\hat{H}$ than the FIGO-TN, while the FIGO-FP are in between. The p-values confirm that FIGO-TP and FIGO-TN have statistically significant different medians for $\hat{H}$, and also show that the median for FIGO-FP $\hat{H}$ is much closer to the median for FIGO-TN $\hat{H}$ than to that of the FIGO-TP $\hat{H}$. Therefore, the time dynamic or variability of the FIGO-TP subjects, as measured by $\hat{H}$, clearly differs from that of the FIGO-TN and the time dynamic or variability, of the FIGO-FP resembles more to that of the FIGO-TN than to that of the FIGO-TP. Fig. 1 also shows that these differences in time dynamic, as measured by $\hat{H}$, are already present 2 to 3 hours before delivery, and that this time dynamic within each class is not significantly varying along time up to three hours before delivery as delivery comes closer, a result that potentially contradict obstetricians intuitions of a smooth decrease of variability when delivery approaches.

A scatter plot of estimated $\hat{H}$ and $\hat{h}_m$ averaged across the last hour before delivery is shown in Fig. 2, together with linear classification performance ROC curve. It shows

satisfactory performance (specificity of 64% for a requested sensitivity of 100%) which outperforms the FIGO classification obtained on the same case study database as reference (specificity of 50% for a sensitivity of 100%) as well as what can be achieved using (STV, LTV) (specificity of 24% for a sensitivity of 100%). Equivalent results are obtained when using 10min long sliding times windows.

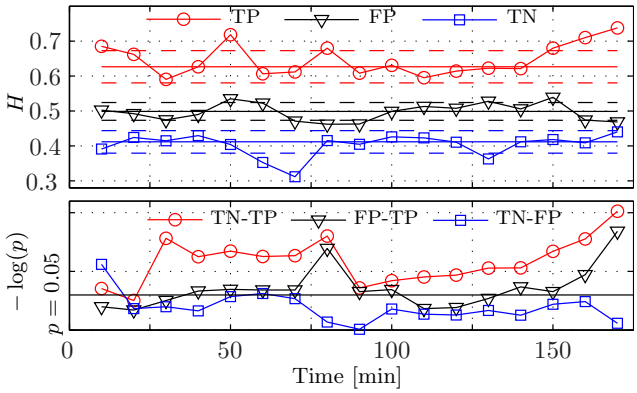

Figure 1: **Time evolution of $\hat{H}$ and discrimination. Top plot: Median of $\hat{H}$ per class (solid line), for each time window , together with the median ± 1SD (dashed line). Bottom plot: Wilcoxon ranksum test p-values, obtained for each time windows, for the 3 pairs of classes.**

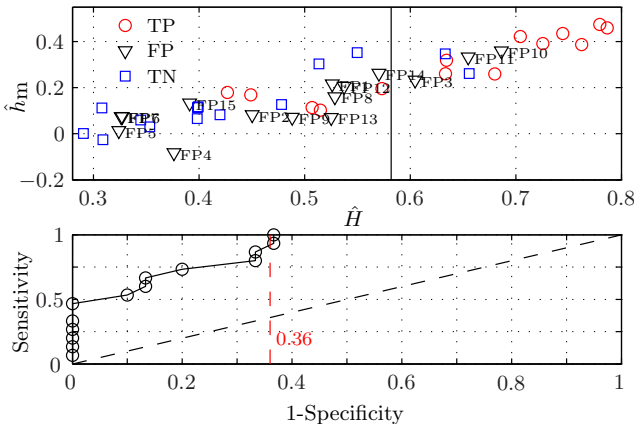

Figure 2: **Scatter plots (top) and ROC curve (bottom)**

4.2 FIGO False Positive case study

Besides global classification performance, the scatter plot in Fig. 2 also enables us to perform a case study of the FIGO-FP with respect to $\hat{H}$ and $\hat{h}_m$. Subjects FIGO-FP 1, 2, 4, 7, 10, 12, 13, 15 are documented as having *low LTV*. Interestingly, 7 out of 8 such subjects are actually taking values of $\hat{H}, \hat{h}_m$ within the range of the FIGO-TN (thus healthy) subjects. Also, subjects FIGO-FP 2, 3, 4, 5, 7, 10, 12, 15 are documented as having *low reactivity*. All but 2 (3 and 10) are are actually taking values of $\hat{H}, \hat{h}_m$ within the range of the FIGO-TN (thus healthy) subjects. This indicates that low LTV and low reactivity actually do not correspond to a change in the scale invariance properties of FHR time series, and thus that the temporal dynamics of such subjects, as measured by H, h_m, actually match that of healthy fetuses. This provides an interesting new perspective of low LTV and low reactivity: Not accompanied by a change of the scaling or temporal dynamics property, it might not be a sign of unhealthy status for the fetus, hence potentially decreasing the number of false positive. Conversely, FIGO-FP 3 and 10 remain misclassified by $\hat{H}, \hat{h}_m$, they are documented as having very high baseline (above 180bpm), which thus may essentially results from a global change of the temporal dynamics and scale invariance properties. Also, FIGO-FP 11 remains misclassified by $\hat{H}, \hat{h}_m$ and FIGO-FP 8, 9 and 14 are very close to the boundary of the healthy domain. These correspond to FIGO-FP subjects documented as having either *variable* or *complicated-shape* decelerations, thus indicating that such decelerations are accompanied by a clear change in the temporal dynamics and scale invariance properties of FHR times series, and hence cannot be discriminated by $\hat{H}, \hat{h}_m$ parameters. This observation motivates the next section that studies in details the relations between scaling and decelerations.

To finish this case study analysis, let us note that most of FIGO-TP are clearly identified as having different $\hat{H}, \hat{h}_m$ and thus different scale invariance properties and temporal dynamics, compared to healthy fetuses. However, a number FIGO-TP have $\hat{H}, \hat{h}_m$ taking values in the healthy range, thus indicating that they were not classified as healthy because of a change in their FHR temporal dynamics but for other reasons.

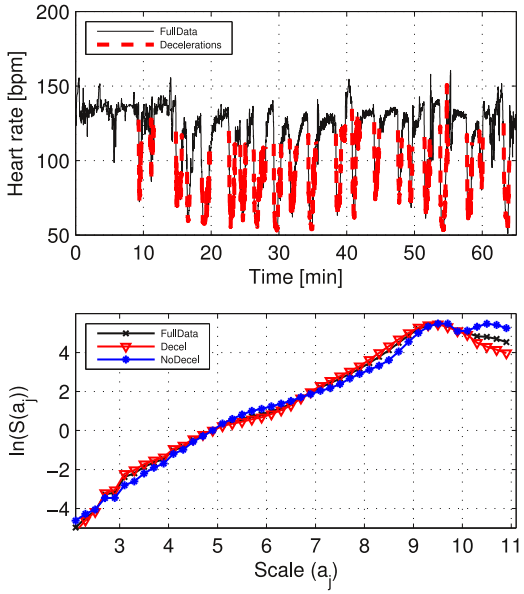

Figure 3: **FHR time series (FIGO-FP14) with automatically detected decelerations (top) and comparison of the wavelet spectrum against the wavelet spectra conditioned to the presence or absence of decelerations.**

4.3 Decelerations versus scale invariance

Automated deceleration detection. To study the relations between decelerations and scale invariance, use is made of an automated baseline evaluation (inspired by [12]), to which an automated deceleration detection has been added by ourselves [6], where decelerations are defined according to FIGO criteria (at least 15 bpm drop of 10s duration). Examples of the output of this automated detection procedure is illustrated in Fig. 3.

Conditional wavelet spectra. Now that decelerations can be detected in an automated manner, their impact on the scaling properties of data can be investigated. To that end, wavelet coefficients are split into two groups, those corresponding to the time occurrences of decelerations, $\{T_X(a,t)\}_{t\in T_D}$ versus those computed at time instant where no decelerations were detected $\{T_X(a,t)\}_{t\in T_{ND}}$ (as illustrated in Fig. 3). Then two different wavelet spectra can be computed, conditional to the occurrence of decelerations or to their absence: $S_D(a) = \frac{1}{n_D}\sum_{k\in T_D} T_X(a,k)^2$ and $S_{ND}(a) = \frac{1}{n_{ND}}\sum_{k\in T_{ND}} T_X(a,k)^2$, and compared, as in Fig. 3.

Decelerations versus scale invariance. First, Fig. 3 shows that, for FHR time series with variable or complicated shape decelerations, the non conditional spectra (computed using all wavelet coefficients) display perfect scaling across the same large range of scales as FHR time series with no or uniform decelerations. Thus, decelerations participate in the same mechanism that produce scale invariance and thus do not correspond to a different temporal dynamics. Second, Fig. 3 clearly shows, that the two conditional wavelet spectra essentially show the same wavelet spectra, at least on the range $a_m = 1s \leq a \leq a^* = 32s$ (corresponding to scales a_j 3 to 7). This means that the two Hurst exponents estimated on the two conditional wavelet spectra are essentially equivalent, therefore, the temporal dynamics of FHR time series during decelerations or in-between decelerations is actually the same in the range of scales $a_m = 1s \leq a \leq a^* = 32s$. These empirical observation shed an interesting light on the relations between decelerations and scale invariance: FIGO-FP and FIGO-TP subjects with variables and complicated shape deceleration are mostly found to have large $\hat{H}$, which betrays a clear changes in the temporal dynamics and scale invariance properties of the FHR time series, that are not caused by decelerations; instead variable or complicated-shape decelerations are rather a manifestation or consequence of one same mechanism that drives the overall change of temporal dynamics and scale invariance properties.

Long term evolution of scale invariance. In the database, there exists a number of very long recordings (several hours), such as FIGO-TP7, shown in Fig. 4. From those, the wavelet spectrum computed in a window of 30 minutes taking place 5 hours before delivery, when almost no decelerations occur, is compared against the wavelet spectrum computed in a window of 30 minutes taking place 40 minutes before delivery, when variable decelerations occur. In addition, conditional wavelet spectra computed from this second time window are also superimposed. Fig. 4 clearly show that 5 hours before delivery this FIGO-TP had a temporal dynamics and scale invariance properties, as measured by $\hat{H}$, that correspond to that of a healthy subject ($\hat{H} = 0.6$), this is no longer the case before delivery when $\hat{H}$ has increased thus showing a significant change in the temporal dynamics towards the non healthy zone ($\hat{H} = 0.79$). For this later block, wavelet spectra conditional to the occurrence or absence of variable decelerations show again the same increased $\hat{H}$ and thus the same temporal dynamics: Variable decelerations are not responsible for the increase in $\hat{H}$; Instead an obvious change in the mechanisms driving time dynamics induces a global change in $\hat{H}$ irrespective of the presence of a deceleration or not as well as the occurrence of variable decelerations.

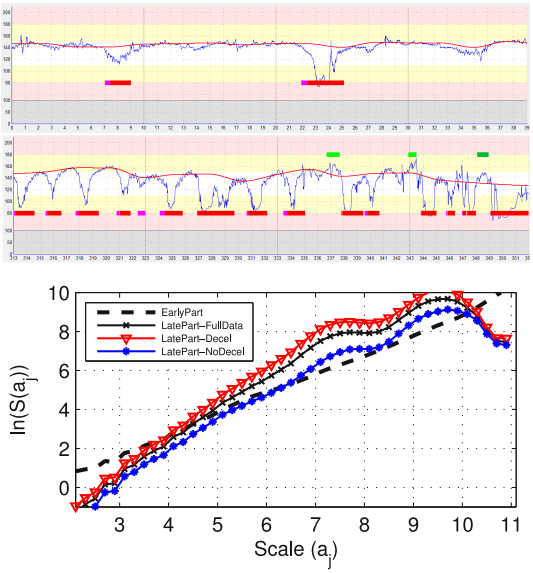

Figure 4: **Long term time variation of $\hat{H}$. Comparisons of the wavelet spectrum, computed from a 6 hour long recording (FIGO-TP7), in two windows of 30 minutes taking place 5 hours and 40 minutes before delivery (above). Wavelet spectrum of early window (black doted line) is plotted against the wavelet spectrum of later window (black solid line), conditional wavelet spectra computed from this second block are also superimposed.**

5 Conclusions and perspectives

It has been explained how fractal (or scale invariance) paradigm reconciles the time variability and spectrum analysis perspectives on FHR times series temporal dynamic of variability, as measured through parameters $\hat{H}, \hat{h}_m$. These parameters can thus be used to characterize different temporal dynamics in intrapartum FHR times series. Also, it is

observed that when departures of parameters $\hat{H}, \hat{h}_m$ from the healthy zone are observed, the departures is usually visible up to 3 hours before delivery. Further, it has been shown that while these two parameters cannot be used alone to achieve perfect classification of intrapartum healthy and non healthy, they enabled us to show that low variability and low reactivity, per se, are not necessarily implying a change in temporal dynamics and hence unhealthy fetuses; Parameters $\hat{H}, \hat{h}_m$ can thus help to classify such cases as healthy and thus to decrease the number of FIGO-FP. Additionally $\hat{H}$ estimation does not require a priori detection of deceleration as is the case when estimating the LTV. Finally, the analysis of the relations between decelerations and scale invariance suggest that changes in $\hat{H}$ and the occurrence of variable and complicated shape decelerations are two manifestations of one same mechanism driving a global and across all scales change in FHR temporal dynamics. In the future, parameters $\hat{H}, \hat{h}_m$ will be used to classify a much larger database and the case study analysis will be extended to other FHR features.

References

[1] P. Abry, P. Gonçalvès, and P. Flandrin. Wavelets, spectrum estimation and $1/f$ processes. In *Wavelets and Statistics, Lecture Notes in Statistics, A. Antoniadis and G. Oppenheim, Eds.*, volume 103, New-York, 1995. Springer-Verlag.

[2] P. Abry, H. Wendt, S. Jaffard, H. Helgason, P. Goncalves, E. Pereira, C. Gharib, P. Gaucherand, and M. Doret. Methodology for multifractal analysis of heart rate variability: From LF/HF ratio to wavelet leaders. *Conf Proc IEEE Eng Med Biol Soc*, 2010:106–109, 2010.

[3] D. Ayres-de Campos, A. Ugwumadu, P. Banfield, P. Lynch, P. Amin, D. Horwell, A. Costa, C. Santos, J. Bernardes, and K. Rosen. A randomised clinical trial of intrapartum fetal monitoring with computer analysis and alerts versus previously available monitoring. *BMC Pregnancy and Childbirth*, page 71, 2010.

[4] M. Cesarelli, M. Romano, and P. Bifulco. Comparison of short term variability indexes in cardiotocographic foetal monitoring. *Comput Biol Med*, 39(2):106–118, Feb 2009.

[5] E. Chandraharan and S. Arulkumaran. Prevention of birth asphyxia: responding appropriately to cardiotocograph (ctg) traces. *Best Pract Res Clin Obstet Gynaecol*, 21(4):609–624, Aug 2007.

[6] V. Chudáček, J. Spilka, L. Lhotská, P. Janku, M. Koucký, M. Huptych, and M. Bursa. Assessment of features for automatic ctg analysis based on expert annotation. *Conf Proc IEEE Eng Med Biol Soc*, 2011:6051–6054, 2011.

[7] G. S. Dawes, M. Moulden, and C. W. Redman. Short-term fetal heart rate variation, decelerations, and umbilical flow velocity waveforms before labor. *Obstet Gynecol*, 80(4):673–678, Oct 1992.

[8] M. Doret, H. Helgason, P. Abry, P. Goncalves, C. Gharib, and P. Gaucherand. Multifractal analysis of fetal heart rate variability in fetuses with and without severe acidosis during labor. *American Journal of Perinatology*, 28(4):259–266, 2011.

[9] F. Esposti, M. G. Signorini, M. Ferrario, and G. Magenes. Self-similarity behavior characterization of fetal heart rate signal in healthy and intrauterine growth retarded fetuses. *Conf Proc IEEE Eng Med Biol Soc*, 1:6157–6160, 2006.

[10] C. S. Felgueiras, J. P. de S, J. Bernardes, and S. Gama. Classification of foetal heart rate sequences based on fractal features. *Med Biol Eng Comput*, 36(2):197–201, Mar 1998.

[11] FIGO. Intrapartum surveillance: recommendations on current practice and overview of new developments. *Int J Gynaecol Obstet*, 49(2):213–221, May 1995.

[12] A. Georgieva, S. J. Payne, M. Moulden, and C. W. G. Redman. Computerized fetal heart rate analysis in labor: detection of intervals with un-assignable baseline. *Physiol Meas*, 32(10):1549–1560, Oct 2011.

[13] H. Helgason, P. Abry, P. Goncalves, C. Gharib, P. Gaucherand, and M. Doret. Adaptive multiscale complexity analysis of fetal heart rate. *IEEE Trans Biomed Eng*, Mar 2011.

[14] P. Hopkins, N. Outram, N. Lofgren, E. C. Ifeachor, and K. G. Rosen. A comparative study of fetal heart rate variability analysis techniques. In *Conf Proc IEEE Eng Med Biol Soc*, pages 1784–1787, 2006.

[15] K. Kiyono, Z. R. Struzik, N. Aoyagi, and Y. Yamamoto. Multiscale probability density function analysis: non-gaussian and scale-invariant fluctuations of healthy human heart rate. *IEEE Trans Biomed Eng*, 53(1):95–102, Jan 2006.

[16] R. F. Leonarduzzi, G. Schlotthauer, and M. E. Torres. Wavelet leader based multifractal analysis of heart rate variability during myocardial ischaemia. In *Conf Proc IEEE Eng Med Biol Soc*, pages 110 –113, 2010.

[17] S. Mallat. *A Wavelet Tour of Signal Processing*. Academic Press, San Diego, CA, 1998.

[18] T. Nakamura, H. Horio, and Y. Chiba. Local holder exponent analysis of heart rate variability in preterm infants. *IEEE Trans Biomed Eng*, 53(1):83–88, Jan 2006.

[19] J. J. Piazze, A. Ruozi-Berretta, A. Cerekja, and M. M. Anceschi. Falsely reassuring short-term variation associated with severe fetal acidemia in a near-term pregnancy. *Int J Gynaecol Obstet*, 87(3):242–244, Dec 2004.

[20] S. Schiermeier, H. Hatzmann, and J. Reinhard. The value of doppler cardiotocogram computer analysis system 70 minutes before delivery. *Z Geburtshilfe Neonatol*, 212(5):189–193, Oct 2008.

[21] M. G. Signorini, G. Magenes, S. Cerutti, and D. Arduini. Linear and nonlinear parameters for the analysis of fetal heart rate signal from cardiotocographic recordings. *IEEE Trans Biomed Eng*, 50(3):365–374, Mar 2003.

[22] J. O. E. H. van Laar, C. H. L. Peters, S. Houterman, P. F. F. Wijn, A. Kwee, and S. G. Oei. Normalized spectral power of fetal heart rate variability is associated with fetal scalp blood ph. *Early Hum Dev*, 87(4):259–263, Apr 2011.

[23] M.-K. Yum, C.-R. Kim, E.-Y. Park, and J.-H. Kim. Instability and frequency-domain variability of heart rates in fetuses with or without growth restriction affected by severe preeclampsia. *Physiol Meas*, 25(5):1105–1113, Oct 2004.